Science and Technology Indonesia
e-ISSN:2580-4391 *p*-ISSN:2580-4405
Vol. 6, No. 3, July 2021

Research Paper

The Ability of Composite Ni/Al-carbon based Material Toward Readsorption of Iron(II) in Aqueous Solution

Normah[1], Neza Rahayu Palapa[3], Tarmizi Taher[2,4], Risfidian Mohadi[3], Hasja Paluta Utami[4], Aldes Lesbani[1,3,4*]

[1]*Magister Programme Graduate School of Mathematics and Natural Sciences, Sriwijaya University, Jl. Padang Selasa No. 524 Ilir Barat 1, Palembang-South Sumatra, Indonesia*
[2]*Departement of Environmental Engineering, Faculty of Mathematics and Natural Sciences, Insitut Teknologi Sumatera, Jl. Terusan Ryacudu, Way Hui, Jati Agung, Lampung 35365, Indonesia*
[3]*Graduate School of Faculty Mathematics and Natural Sciences, Sriwijaya University, Jl. Padang Selasa No. 524 Ilir Barat 1, Palembang-South Sumatra, Indonesia*
[4]*Research Center of Inorganic Materials and Coordination Complexes, Faculty of Mathematics and Natural Sciences, Universitas Sriwijaya, Jl. Palembang Prabumulih Km.32 Ogan Ilir 30662, Indonesia*
***Corresponding author**: aldeslesbani@pps.unsri.ac.id

Abstract
In this research, NiAl-LDH was synthesized using the coprecipitation method and modified with biochar and graphite to produce NiAl-biochar and NiAl-graphite composite materials. The adsorbent that has been synthesized is used for the application of adsorption of Fe(II) ions in aqueous solution. The resulting material was characterized by XRD (X-ray Diffraction) analysis, spectrophotometer FT-IR, BET analysis for determine the specific surface area and TG-DTA analysis. XRD diffractogram showed that the NiAl-Biochar and NiAl-graphite composite material had the diffraction pattern characteristic of the precursor. LDH that has been modified will have a larger surface area than the precursor. The surface area of NiAl-biochar reaches 438.942 m^2/g and the surface area of NiAl-graphite reaches 21.595 m^2/g. This composite material supports adsorbents with a large adsorption capacity to adsorb metals. Adsorption of Fe (II) using NiAl-Biochar and NiAl-graphite was stable for five regeneration cycles (<75.30%). The Fe(II) ion adsorption process tends to follow the Langmuir isotherm model which has a maximum capacity value (Qmax) of NiAl-Biochar composite material reaching 20 times with a value of 243.902 mg/g and the NiAl-graphite composite reaching 72.464 mg/g, so that the carbon-based composite material is considered effective. adsorbent to remove Fe(II) ion and can increase the stability of the structure for adsorption regeneration. The results of the analysis of thermodynamic parameters showed that the adsorption process was endothermic, took place spontaneously and the solid-liquid phase interface increased according to the increasing degree of disorder.

Keywords
Layered Double Hydroxide, Composite, Biochar, Graphite, Iron

Received: 22 March 2021, Accepted: 13 June 2021
https://doi.org/10.26554/sti.2021.6.3.156-165

1. INTRODUCTION

LDHs are a class of anionic clays or hydrotalcite (Hu et al., 2019a). The layered structure of LDH is based on a sheet like brucite which has a positive charge on the surface of the layer and a negative charge between the layers due to the presence of anions and water molecules (Cao et al., 2016). LDHs have the formula $[M^{2+}_{(1-x)}M^{3+x}(OH)_2]^{x+}[A^{n-}_{x/n}.mH_2O]$ where M^{2+} and M^{3+} is a divalent metal ion and trivalent metal ion. A^{n-} indicates organic or inorganic anions with n- valence (Hu et al., 2019a). In addition, LDH has been known for more than 150 years for its distinctive 2D flat structure and has studied many of the most advanced functional materials used in materials, energy sciences and environmental (Cao et al., 2016). LDH has many interesting properties, such as compositional flexibility (Taher et al., 2019), anion exchange (Lesbani et al., 2021), biocompatibility (Cao et al., 2016), high porosity and surface area (dos Santos Lins et al., 2019). Such structure and characteristics give wide application of LDH as a catalyst (Hu et al., 2019b), adsorbent (Lesbani et al., 2021) and ion exchanger (Gascho et al., 2019).

Recently, LDHs have been studied to remove organic, inorganic and heavy metal pollutants. The application of LDH as an adsorbent agent has several drawbacks such as a difficult regeneration process because it can undergo exfoliation (dos Santos Lins et al., 2019) and aggregate formation which limits its widespread use (Tan et al., 2019). Therefore, its use is more effective as a composite by adding supporting material to increase layer integrity, such as activated carbon (dos Santos Lins et al., 2019), biochar (Tan et al., 2019) and graphite

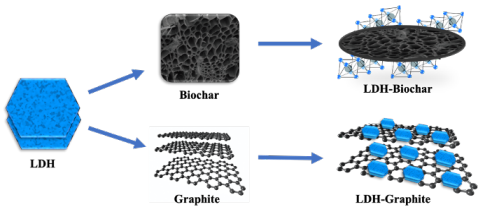

Figure 1. Schematic illustration of preparing the composite LDH-Biochar and LDH-Graphite

(Lee et al., 2018). As introduced, biochar and graphite are attractive materials with interesting properties.

According to Lesbani et al. (2021) biochar is one of the promising supporting materials as an LDH matrix. Organic compounds or biomass are produced through a pyrolysis process that uses high temperatures. The porous biochar acts as an ideal support matrix providing a large reactive area for effective metal hydroxide decoration (Zubair et al., 2017). According to Tan et al. (2019) LDH can be made into a composite by combining two different materials and supporting material in the form of biochar and can improve the ability and adsorption properties to remove pollutants. Apart from that, graphite can also be combined with LDH. In recent years, graphite is considered to be a very efficient adsorbent. Linghu et al. (2017a) reported that LDH/graphite composites can be used as excellent adsorbents. The graphite contribution in the composites significantly improves its adsorption performance. According to Hu et al. (2020) layered double hydroxides composite with carbon support can effectively prevent agglomeration and increase the specific surface area of the adsorbent produced to provide more active sites to improve the adsorption performance to remove pollutants.

Based on research by Hu et al. (2020) the surface area of Ni/Fe-carbon composites has doubled to reach 232 m^2/g, while Ni/Fe LDH has a surface area of 108 m^2/g. According to Wang et al. (2016) reported the large specific surface area of LDH/carbon composites can increase the adsorption capacity to remove As(V) metal from 156 mg/g to 438 mg/g. According to Tyas et al. (2018) the ability to regenerate is more stable with composite materials. Alagha et al. (2020) reported that biochar-Mg/Al composites have the potential for repeated use in the phosphate adsorption process and the regeneration process has decreased which is not too significant after five cycles of 92%.

In this study, NiAl-LDH was composited with biochar and graphite using the coprecipitation method which resulted in NiAl-Biochar and NiAl-graphite composites. The material is applied as an adsorbent to remove Fe(II) ion contaminants. The prepared materials were characterized using XRD, FT-IR, BET and TG-DTA analysis. Application as an adsorbent, this research carried out the adsorption process with regeneration studies and adsorption was carried out with isotherm and thermodynamic parameters.

2. EXPERIMENTAL SECTION

2.1 Material

The precursors $Al(NO_3)_3 \cdot 9H_2O$ 99% (aluminum nitrate nonahydrate), $FeCl_2.4H_2O$ 99% (iron(II) chloride), $Ni(NO_3)_2 \cdot 3H_2O$ 99% (nickel nitrate trihydrate), NaOH 99% (sodium hydroxide), and HCl 37% (hydrochloric acid) were purchased from Merck and Sigma-Aldrich. All precursors were utilized as received without further purification. In this study, rice husks obtained from rice mills are used as a precursor for biochar and graphite by Bukataorganics Indonesian. Material characterization was carried out with X-ray Diffraction Rigaku miniflex-6000. Material is scanned from 5-80° with a scanning speed of 1°/min. Materials were analyzed using FT-IR Shimadzu Prestige-2 and using KBr pellets at wavenumbers around 400-4000 cm^{-1}. Adsorption-desorption of N_2 was carried out using Quantachrome Micrometic ASAP to determine the pore volume, pore diameter and specific surface area of the material. Analysis of Fe(II) ion concentration complexed with 1,10-phenanthroline and analyzed using a spectrophotometer 1800 PC UV-Visible Biobase BK-UV Spectrophotometer with a wavelength at a maximum absorbance of 513 nm.

2.2 Methods

2.2.1 Synthesis NiAl-LDH

Synthesis of NiAl-LDH by coprecipitation method (Kovalenko et al., 2017). 100 mL of $Ni(NO_3)_2 \cdot 3H_2O$ (0.75 M) solution mixed with 100 mL of $Al(NO_3)_3 \cdot 9H_2O$ (0.25 M) (molar ratio 3:1) in a beaker. The mixture was added 50 mL of 2 M NaOH until it reached pH 10. The mixture was stirred until homogeneous and kept for 20 hours at a temperature of 80°C until a precipitate was formed. Then filtered using a vacuum, rinsed with distilled water, and dried at 110°C to dry.

2.2.2 Preparation of Composite NiAl-Biochar LDH

The synthesis of NiAl-Biochar LDH composites was made using the coprecipitation method (Palapa et al., 2020c) carried out with (Lesbani et al., 2021) 10 mL $Ni(NO_3)_2 \cdot 3H_2O$ (0.75 M) solution was mixed with 10 mL $Al(NO_3)_3 \cdot 9H_2O$ (0.25 M) and stirred until homogeneous. The resulting mixture was stirred and added with 1 g of biochar from the rice husk precursor. The mixture was added with 2 M NaOH until it reached pH 10. The solution mixture was stirred and kept for 3 days at 80°C. The composite was filtered, rinsed, and dried at 40°C to dryness.

2.2.3 Preparation of Composite NiAl-Graphite LDH

The method is the same as for the preparation of NiAl-Biochar composites (Cao et al., 2016). 10 mL $Ni(NO_3)_2 \cdot 3H_2O$ (0.75 M) solution and 10 mL $Al(NO_3)_3 \cdot 9H_2O$ (0.25 M) were mixed and stirred until homogeneous. The resulting mixture was added with 2 M of NaOH until it reached pH 10 and added with 1 g of graphite. The mixture was treated in the same way as the NiAl-Biochar composite.

2.2.4 Batch adsorption studies

Adsorption studies through the regeneration process, isotherm and thermodynamic parameters. Firstly, regeneration is carried out using an ultrasonic instrument. Adsorption of 20 mL of 100 mg/L of Fe(II) solution, plus 0.2 g of adsorbent and shaker for 3 hours. After the adsorption process, the desorption process is carried out using water. The desorption process was carried out with the adsorbent that had been used for the adsorption process and 0.01 g was taken, each added 10 mL of reagent and shaken for 2 hours. The regeneration process uses used adsorbents. The solution was measured using a UV-Vis spectrophotometer after being complexed with 1,10-phenanthroline. The regeneration process is carried out in seven cycles with the same procedure. Secondly, the isotherm and thermodynamic parameters of the adsorption were carried out with an initial concentration of 20 mL of Fe (II) solution (10-50) mg/L, with the addition of 0.02 g of adsorbent and shaken for 120 minutes and using a variation of the adsorption temperature (30, 40, 50, and 60°C). Third, the Fe(II) solution is mixed with Ni(II) metal with a concentration of 10 mg/L then adsorbed with time variations of 200 minutes. The final concentration of Fe(II) was analyzed at a wavelength of 513 nm using a UV-Vis Spectrophotometer after being complexed with 1,10-phenanthroline.

3. RESULTS AND DISCUSSION

3.1 Characterization of the adsorbent

XRD was used to analysis the structure of the material obtained. The XRD patterns of NiAl-LDH, Biochar, NiAl-Biochar and Graphite, and NiAl-Graphite are shown in Figure 2. The XRD patterns of NiAl-LDH in Figure 2 (a) show indications of hydrotalcite according to JCPDS No.15-0087 (Wang et al., 2016). A typical principal diffraction peak is seen at 2θ = 11.7°, 23.5°, 35.1°, 39.7°, 47.3°, 61.2°, and 62.5° correspond to the crystal plane (003), (006), (012), (015), (018), (110) and (113) from NiAl-LDH, ensuring that the synthesis of NiAl-LDH is successful (Hu et al., 2019a). The XRD pattern of Biochar in Figure 2(b) shows that Biochar has an angle of 2θ = 23°(002). (Mon, 2018) reported that the diffraction peaks in Biochar were wide, indicating that biochar has amorphous silica. Figure 2(c) shows the NiAl-Biochar pattern associated with NiAl-LDH with a diffraction angle of 11.60° and a biochar relationship with a diffraction angle of 23°. According to (Tan et al., 2019) the NiAl-Biochar composite pattern has a decreased intensity due to the amorphous nature of biochar.

Figure 2(d) shows a graphite diffractogram. According to Gascho et al. (2019) graphite has two characteristic peaks at 2θ = 26° (002) and 55° (004). In the graphite pattern Figure 2(d) only has a peak (002) at 2θ = 26° (Gascho et al., 2019) and graphite has high crystallinity with a high peak sharp (Kusrini et al., 2019). NiAl-Graphite is presented in Figure 2(e) which shows that the NiAl-Graphite pattern resembles the characteristics of NiAl-LDH and graphite. The XRD NiAl-Graphite pattern has a peak at 2θ = 12° which shows the characteristics

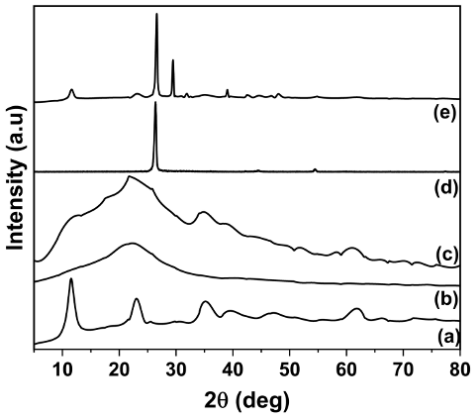

Figure 2. XRD powder patterns of NiAl-LDH (a), Biochar (b), NiAl- Biochar (c), Graphite (d), and NiAl- Graphite (e)

of NiAl-LDH and a peak at 2θ = 26° which shows the characteristics of graphite. The pattern of NiAl-Graphite composite shows high intensity which indicates that the material has high crystallinity due to the properties of graphite.

The results of FT-IR analysis of NiAl-LDH, Biochar, NiAl-Biochar, Graphite and NiAl-Graphite are shown in Figure 3. The NiAl-LDH spectrum is shown in Figure 3(a), according to Ravuru et al. (2019) wide peak at 3448 cm^{-1} shows the O-H strain of surface hydroxyl groups and water molecules between layers. The peak with 1381 cm^{-1} is caused by stretching and vibration of NO_3^-. Vibration corresponding to 1635 cm^{-1} indicates O-H bending. peaks at 794 cm^{-1} and 587 cm^{-1} each vibration to M-O and O-M-O. Figure 3(b) shows the spectrum of biochar. The peak at 3448 cm^{-1} is thought to originate from the strain vibration of the hydroxyl group. The 2368 cm^{-1} peak shows the C-C strain vibration. The peaks correspond to the aliphatic $-CH_2$ strain vibration and significant C=C aromatic peaks appearing at 1095 cm^{-1} and 798 cm^{-1} (Palapa et al., 2020b). Figure 3(c) shows the NiAl-Bichar spectrum. The peaks appear at 3448 cm^{-1}, 2368 cm^{-1}, 1635 cm^{-1}, 1381 cm^{-1}, 1095 cm^{-1} and 798 cm^{-1}. All peaks that appear on NiAl-Biochar are NiAl-LDH and biochar vibrations. The graphite spectrum is shown in Figure 3(d). According to Linghu et al. (2017a) peaks at 3432 cm^{-1} showed O-H vibrations. A peak at 1614 cm^{-1} is associated with aromatic C=C and a peak at 1381 cm^{-1} indicates a stretch of C=O in the carboxylic acid group (Linghu et al., 2017b). Figure 3(e) NiAl-Graphite spectrum appears peaks of 3448 cm^{-1}, 1614 cm^{-1}, 1381 cm^{-1}, 794 cm^{-1} showing NiAl-LDH and graphite vibrations.

The BET isotherm is presented in Figure 4. From the figure, it can be seen that the shape of the isotherm is similar to the type IV which is indicated by the presence of a hysteresis loop. This indicates that the gas capillary condensation in the mesopore at relatively high pressure. Loop hysteresis shows H2-type in the presence of bottle-shaped pores with a narrow mouth and a wide body (Ravuru et al., 2019).

The isotherm data are shown in Table 1. Table 1 shows

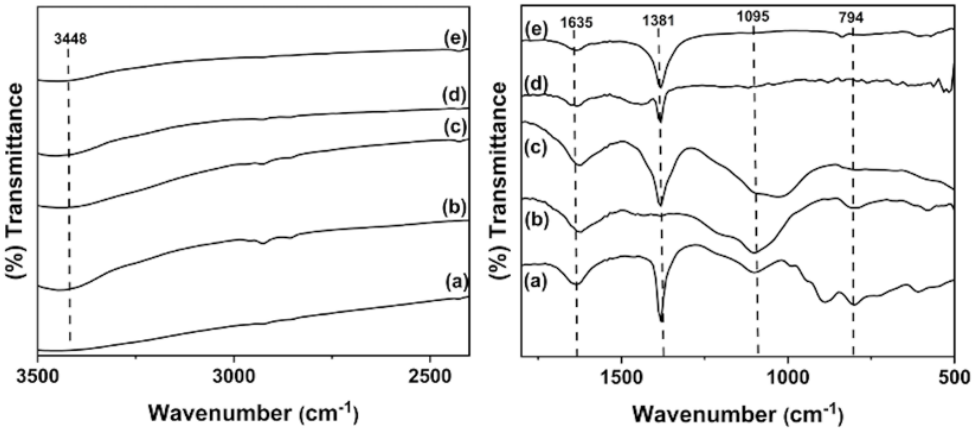

Figure 3. FTIR spectrum of NiAl LDH (a), Biochar (b), NiAl-Biochar (c), Graphite (d), and NiAl- Graphite (e)

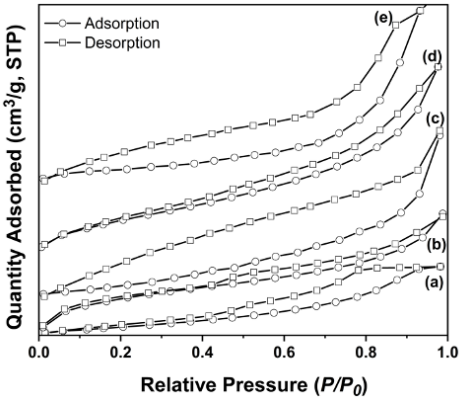

Figure 4. BET profile of NiAl LDH (a), Biochar (b), NiAl-Biochar (c), Graphite (d), and NiAl- Graphite (e)

that NiAl-biochar and NiAl-graphite have a larger surface area compared to NiAl-LDH, biochar and graphite. NiAl-Biochar has a specific surface area of 438.942 m^2/g and NiAl-graphite of 21.595 m^2/g. NiAl-biochar surface area has a surface area twenty times that of NiAl-Graphite. This is because biochar and graphite can prevent agglomeration and increase the specific surface area (Lyu et al., 2020).

The thermal behavior of NiAl-LDH, biochar, graphite, NiAl-biochar and NiAl-graphite carried out with nitrogen is presented in Figure 5. It can be seen from Figure 5 (a) which shows that NiAl-LDH has two endothermic peaks at 90°C which shows loss of nitrates and loss of air molecules. The peak was at 300°C indicating that NiAl-LDH lost water molecules on the interlayer. Figure 5 (b) shows the fact of mass reduction at 400°C and at 600°C which shows the decomposition of lignin. The decrease in landmass which reaches 800°C is insignificant degradation occurs because most of the volatile molecules have undergone pyrolysis (Wazir et al., 2020). Figure 5 (c) shows one endothermic peak at 430°C and 510°C which indicates that LDH decomposition and oxidation of the biochar material occurs. Figure 5 (d) shows that at a temperature of 760°C the graphite material has become graphite oxide. Figure 5 (e) has an endothermic peak at 90°C which indicates a loss of water molecules, a peak at 800 °C indicating that there has been a change to oxides.

3.1.1 Adsorption

The results of Fe(II) ion adsorption regeneration using NiAl LDH, Biochar, NiAl-Biochar, Graphite, and NiAl-Graphite showned in Figure 6 were carried out seven times. The results showed that the NiAl-biochar and NiAl-Graphite composite materials had a greater adsorption capacity and a more stable regeneration process compared to pure materials. Adsorption of Fe(II) ion using NiAl-Biochar and NiAl-graphite was stable for five regeneration cycles, respectively reaching 91.08%-77.26% and 83.11%-75.30%. this is because the process of modifying LDH with carbon-based materials can increase the stability of the structure (Alagha et al., 2020). The figure shows that NiAl-biochar material has a greater adsorption capacity than NiAl-graphite, this is supported by BET analysis data which shows NiAl-biochar has a larger specific surface area. The adsorption capacity of NiAl-LDH, Biochar and graphite has decreased significantly in the regeneration process, this is because the material has an unstable structure which results in exfoliation when used repeatedly (Palapa et al., 2020d) and structural damage. So it can be concluded that LDH modification with carbon-based materials can improve the stability of the LDH structure (Tang et al., 2020).

Thermodynamic parameters were studied through variations in the initial concentration of Fe(II) ions and the adsorption temperature as shown in Figure 7. Figure 7 shows that the adsorption capacity increases with increasing adsorption temperature used. It can be seen that the adsorption temperature greatly affects the maximum adsorption capacity for Fe(II) ions, this is because the increase in temperature causes an increase in the number of active sites on the surface and there is an increasing number of interactions between Fe(II) ions and active sites (Dada et al., 2017).

Table 1. NiAl-LDH performance with different support materials

Materials	Specific Surface Area (m^2/g)	Pore Diameter (nm)BJH	Pore Volume (cm^3/mg)BJH
NiAl-LDH	15.106	2.897	0.043
Biochar	50.936	12.089	0.025
Graphite	11.558	3.169	0.027
NiAl-Biochar	438.942	12.301	0.002
NiAl-Graphite	21.595	3.153	0.034

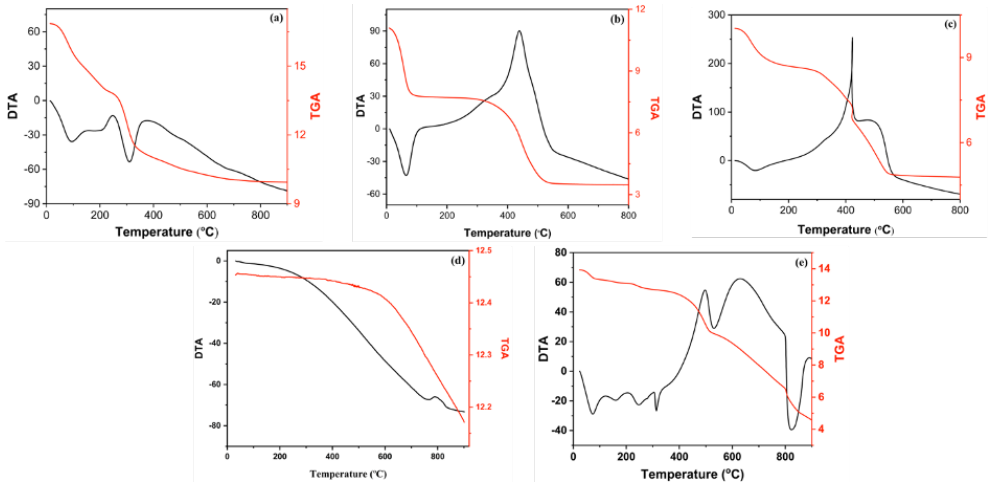

Figure 5. Thermal profile of NiAl-LDH (a), Biochar (b), NiAl- Biochar (c), Graphite (d), and NiAl-Graphite (e)

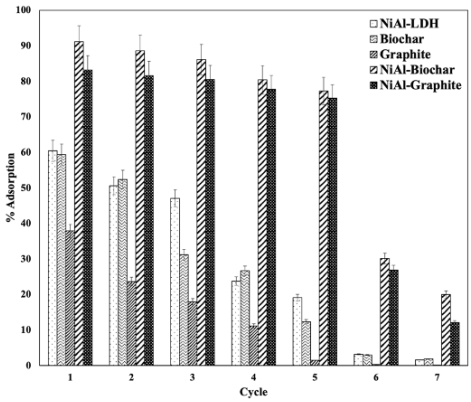

Figure 6. Regeneration Fe(II) on NiAl LDH, Biochar, NiAl-Biochar, Graphite, and NiAl-Graphite

Table 2 shows the results of the calculation of the adsorption isotherm. According to Siregar et al. (2021) isotherm parameters are obtained from the equations of Langmuir and Freundlich. Table 2 shows that the highest value of adsorption capacity (Qmax) in NiAl-Biochar composite material reaches 243.902 mg/g at a temperature of 333 K and NiAl-graphite composite reaches 72.464 mg/g, so carbon-based composite materials are considered as an effective adsorbent to remove the Fe(II) ion. The adsorption capacity of NiAl-biochar and NiAl-graphite has a larger adsorption capacity compared to pure materials, this is supported by the larger surface areas of NiAl-biochar and NiAl-graphite. The larger the surface area, the more active sites available on the surface will increase the performance of the material in the adsorption process (Hu et al., 2020).

The determination of the adsorption isotherm model is seen from the linear regression value which is closer to the value 1. From the data in Table 2 it can be seen that the isotherm model for each adsorbent tends to approach the Langmuir isotherm model with a linear regression value $R^2 > 0.997$. According to Edet and Ifelebuegu (2020), the Langmuir model explains that monolayer adsorption at different active sites, means that there is no transmigration of the adsorbate in the surface area and assumes a uniform monolayer absorption energy to the adsorbent surface. Dada et al. (2017) assume that in the Langmuir isotherm model there is no interaction between adsorbed adjacent species, the adsorption process only occurs at certain locations located on the active surface site.

The adsorption capacity of several adsorbents to remove Fe(II) metal ions, as well as the adsorbent synthesized in the form of NiAl-LDH, biochar, graphite, NiAl-biochar and NiAl-graphite used in this study is presented in Table 3. The adsorption capacity of NiAl-LDH composite materials with carbon-

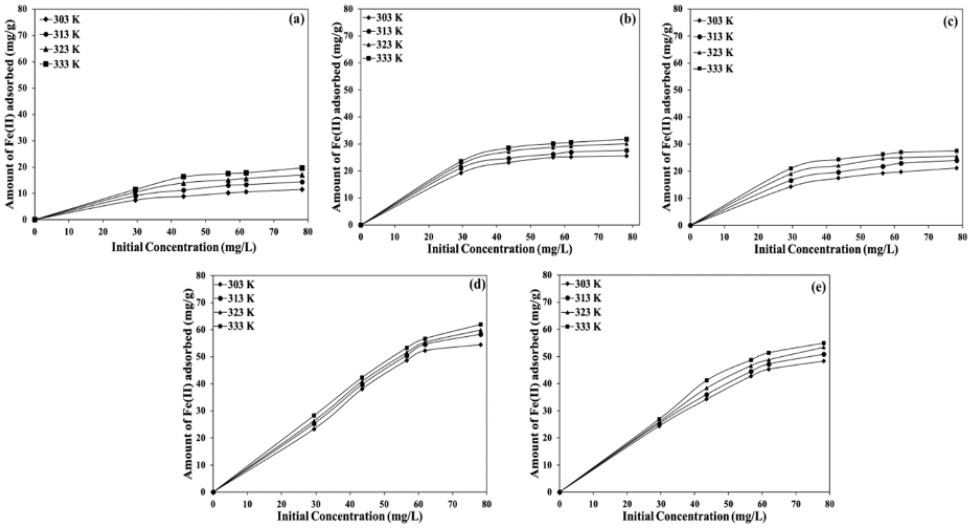

Figure 7. Effect of Fe(II) concentration on Ni/Al LDH (a), Biochar (b), Graphite (c), NiAl-Biochar (d), and Ni/Al-Graphite (e)

Table 2. Isotherm model of Fe(II) adsorption on Ni/Al LDH, Biochar, Ni/Al- Biochar, Graphite, and Ni/Al-Graphite

LDH	Adsorption Isotherm	Adsorption Constant	T(K)			
			303 K	313 K	323 K	333 K
NiAl-LDH	Langmuir	Q_{max}	25.907	28.986	29.07	29.586
		kL	0.078	0.09	0.17	0.272
		R^2	0.998	0.998	0.997	0.999
	Freundlich	n	3.092	3.494	4.456	5.811
		kF	5.976	7.963	11.241	14.639
		R^2	992	0.997	0.993	0.996
Biochar	Langmuir	Q_{max}	27.855	29.499	31.847	33.333
		kL	0.242	0.284	0.34	0.38
		R2	0.999	0.999	0.999	0.999
	Freundlich	n	4.615	5.838	5.807	6.317
		kF	11.768	14.727	16.237	17.968
		R^2	0.979	0.993	0.967	0.965
Graphite	Langmuir	Q_{max}	16.026	20.161	23.095	20.534
		kL	0.038	0.04	0.046	0.061
		R2	0.996	0.997	0.992	0.976
	Freundlich	n	2.409	2.183	2.225	2.078
		kF	2.067	2..282	2.856	3.02
		R^2	0.998	0.995	0.946	0.889
NiAl-Biochar	Langmuir	Q_{max}	83.333	86.207	90.909	243.9
		kL	0.033	0.208	0.029	0.266
		R^2	0.992	0.898	0.95	0.996
	Freundlich	n	1.029	1.196	1.75	2.743
		kF	5.766	10.361	18.88	32.367
		R^2	0.934	0.953	0.952	0.711
NiAl-Graphite	Langmuir	Q_{max}	57.803	61.728	62.5	72.464
		kL	0.056	0.046	0.068	0.148
		R^2	0.991	0.994	0.993	0.992
	Freundlich	n	1.745	2.053	2.293	3.403
		kF	2.616	3.963	5.349	25.864
		R^2	0.995	0.989	0.891	0.932

Table 3. Comparison of the adsorption capacity of Fe(II) metal ions with various adsorbents

Adsorbent	Adsorption Capacity (mg/g)	Reference
Carbon-MgAl LDH	80	(Kundu and Naskar, 2021)
Ca/Al LDH	11.16	(Taher et al., 2019)
Ca/Al-[α-$SiW_{12}O_{40}$]	11.93	(Taher et al., 2019)
Thiourea Cross-Linked Chitosan	48.3	(Dai et al., 2012)
Chitosan	28.7	(Radnia et al., 2012)
Co/Mo LDH	10	(Mostafa et al., 2014)
Rice Husk Ash	6.211	(Zhang et al., 2014)
Banana Peel	33.79	(Shrestha, 2018)
Ni/Al LDH intercalated with keggin ion	36.49	(Lesbani et al., 2020)
Bentonite	7.09	(Al-Shahrani, 2013)
NiAl-LDH	29.586	This Research
Biochar	33.333	This Research
Graphite	23.095	This Research
NiAl-Biochar	243.902	This Research
NiAl-Graphite	72.464	This Research

based materials has capacity which is greater compared to NiAl-LDH before modification. NiAl-Biochar composites have an adsorption capacity of up to two times compared to NiAl-Graphite. This is supported by large data on the surface area of the NiAl-Biochar material, therefore NiAl-Biochar has more active site interactions with Fe(II) metal ions on the adsorbent surface.

In adsorption studies the effect of temperature is an important parameter, this is because several important thermodynamic parameters can be determined such as ΔH (enthalpy), ΔS (entropy) and ΔG (Gibbs free energy). The adsorption temperature used in this study was from 303K-333K. Based on the research of Palapa et al. (2020a) thermodynamic results were calculated by The Van't Hoff equation.

Table 4 assumes that the adsorption occurs endothermically because it has a positive ΔH value (ΔH = +13,677-25,919 kJ/mol) and ΔH<84 kJ/mol assumes that the adsorption process occurs by physical adsorption. The ΔS value is positive (0.052-0.091 J/mol.K) which assumes the degree of irregularity at the solid-liquid interface during the adsorption process of Fe(II) ion onto the adsorbent surface. the adsorption and desorption processes occur simultaneously in the adsorption process, so the increase in the irregularity of the adsorbate molecules is associated with a dissociative process where during bond breaking (desorption) the energy absorbed is greater than the energy released during bond formation (adsorption). Thus, a positive ΔS value indicates that the Fe(II) ion has a high affinity for the adsorbent, this is because the energy required to break the same bond is greater than the energy required to form a bond with the adsorbent (Antonelli et al., 2020). According to Lafi et al. (2018) negative values on free energy Gibbs (ΔG) assume that viability, feasibility, spontaneity of adsorption process and adsorbate have high affinity for adsorbents. In addition, according to Antonelli et al. (2020) with increasing temperature in the adsorption process, the value of G decreases, it indicates that the adsorption process is better carried out at higher temperatures.

4. CONCLUSIONS

In this study, NiAl-Biochar and NiAl-Graphite composite materials were successfully synthesized and NiAl-LDH, Biohar, graphite, NiAl-Biochar and NiAl-graphite were applied as an adsorbent to reduce the levels of Fe(II) metal ions in aqueous solution. The resulting material was characterized and analyzed using XRD analysis, analysis using FT-IR spectrophotometer, BET analysis and TG-DTA analysis to see from the start. Characterization using BET showed that the surface area of NiAl-biochar and NiAl-graphite composites increased as precursors. The surface areas of NiAl-Biochar and NiAl-graphite reached 438.942 m^2/g and 21.595 m^2/g. This composite material supports adsorbents with a large adsorption capacity to adsorb metals. Adsorption of Fe(II) ion using NiAl-Biochar and NiAl-graphite was stable for five regeneration cycles <75.30%. The adsorption of Fe(II) ions on the prepared adsorbent tend to follows the Langmuir adsorption isotherm model with a maximum capacity (Qmax) of the NiAl-Biochar composite material reaching 243.902 mg/g and the NiAl-graphite composite reaching 72.464 mg/g, so carbon-based composite materials are considered effective. adsorbent to remove Fe(II) ions and can increase the stability of the structure for adsorption regeneration. Thermodynamic data results analysis of the adsorption process occurred endothermic, spontaneously and the degree of irregularity increased in the solid-liquid phase interface.

Table 4. Thermodynamic parameters of Fe(II) adsorption on Ni/Al LDH, Biochar, Ni/Al- Biochar, Graphite, and Ni/Al-Graphite

Adsorbent	T (K)	Qe (mg/g)	ΔH (kJ/mol)	ΔS (J/mol.K)	ΔG (kJ/mol)
NiAl-LDH	303	15.29	25.919	0.091	-1.545
	313	16.603			-2.451
	323	19.079			-3.358
	333	21.093			-4.264
Biochar	303	19.27	20.487	0.073	-1.624
	313	21.093			-2.354
	323	22.426			-3.084
	333	23.515			-3.813
Graphite	303	7.488	17.712	0.066	-2.373
	313	9.066			-3.036
	323	10.426			-3.699
	333	11.515			-4.362
NiAl-Biochar	303	24.385	21.259	0.083	-3.867
	313	25.297			-4.697
	323	25.964			-5.526
	333	26.916			-6.355
NiAl-Graphite	303	54.476	13.677	0.052	-2.16
	313	58.359			-2.683
	323	59.946			-3.206
	333	61.932			-3.728

5. ACKNOWLEDGEMENT

Thanks to Sriwijaya University through the Hibah Profesi No.150/SP2H/LT/DRPM/2021 and thanks to the Laboratory of Inorganic Materials and Complexes of the Faculty of Mathematics and Natural Sciences, Sriwijaya University.

REFERENCES

Al-Shahrani, S. (2013). Treatment of wastewater contaminated with Fe (II) by Adsorption onto Saudi Activated Bentonite. *International Journal of Engineering & Technology*, **13**(06); 1–12

Alagha, O., M. S. Manzar, M. Zubair, I. Anil, N. D. Mu'azu, and A. Qureshi (2020). Comparative Adsorptive Removal of Phosphate and Nitrate from Wastewater Using Biochar-MgAl LDH Nanocomposites: Coexisting Anions Effect and Mechanistic Studies. *Nanomaterials*, **10**(2); 336

Antonelli, R., G. R. P. Malpass, M. G. C. da Silva, and M. G. A. Vieira (2020). Adsorption of ciprofloxacin onto thermally modified bentonite clay: Experimental design, characterization, and adsorbent regeneration. *Journal of Environmental Chemical Engineering*, **8**(6); 104553

Cao, Y., G. Li, and X. Li (2016). Graphene/layered double hydroxide nanocomposite: Properties, synthesis, and applications. *Chemical Engineering Journal*, **292**; 207–223

Dada, A. O., F. A. Adekola, and E. O. Odebunmi (2017). Kinetics, mechanism, isotherm and thermodynamic studies of liquid phase adsorption of Pb2 onto wood activated carbon supported zerovalent iron (WAC-ZVI) nanocomposite. *Cogent Chemistry*, **3**(1); 1351653

Dai, J., F. Ren, and C. Tao (2012). Adsorption Behavior of Fe(II) and Fe(III) Ions on Thiourea Cross-Linked Chitosan with Fe(III) as Template. *Molecules*, **17**(4); 4388–4399

dos Santos Lins, P. V., D. C. Henrique, A. H. Ide, C. L. de Paiva e Silva Zanta, and L. Meili (2019). Evaluation of caffeine adsorption by MgAl-LDH/biochar composite. *Environmental Science and Pollution Research*, **26**(31); 31804–31811

Edet, U. A. and A. O. Ifelebuegu (2020). Kinetics, isotherms, and thermodynamic modeling of the adsorption of phosphates from model wastewater using recycled brick waste. *Processes*, **8**(6); 665

Gascho, J. L. S., S. F. Costa, A. A. C. Recco, and S. H. Pezzin (2019). Graphene Oxide Films Obtained by Vacuum Filtration: X-Ray Diffraction Evidence of Crystalline Reorganization. *Journal of Nanomaterials*, **2019**; 1–12

Hu, H., S. Wageh, A. A. Al-Ghamdi, S. Yang, Z. Tian, B. Cheng, and W. Ho (2020). NiFe-LDH nanosheet/carbon fiber nanocomposite with enhanced anionic dye adsorption performance. *Applied Surface Science*, **511**; 145570

Hu, X., P. Li, X. Zhang, B. Yu, C. Lv, N. Zeng, J. Luo, Z. Zhang, J. Song, and Y. Liu (2019a). Ni-based catalyst derived from NiAl layered double hydroxide for vapor phase catalytic exchange between hydrogen and water. *Nanomaterials*, **9**(12); 1688

Hu, Z., L. Cai, J. Liang, X. Guo, W. Li, and Z. Huang (2019b).

Green synthesis of expanded graphite/layered double hydroxides nanocomposites and their application in adsorption removal of Cr (VI) from aqueous solution. *Journal of Cleaner Production*, **209**; 1216–1227

Kovalenko, V., V. Kotok, A. Yeroshkina, and A. Zaychuk (2017). Synthesis and characterisation of dyeintercalated nickelaluminium layereddouble hydroxide as a cosmetic pigment. *Eastern-European Journal of Enterprise Technologies*, **5**(12 (89)); 27–33

Kundu, S. and M. K. Naskar (2021). Carbon-layered double hydroxide nanocomposite for efficient removal of inorganic and organic based water contaminants – unravelling the adsorption mechanism. *Materials Advances*, **2**(11); 3600–3612

Kusrini, E., A. A. Suhrowati, A. Usman, D. V. Degirmenci, and M. Khalil (2019). Synthesis and Characterization of Graphite Oxide, Graphene Oxide and Reduced Graphene Oxide from Graphite Waste using Modified Hummers's Method and Zinc as Reducing Agent. *International Journal of Technology*, **10**(6); 1093

Lafi, R., I. Montasser, and A. Hafiane (2018). Adsorption of congo red dye from aqueous solutions by prepared activated carbon with oxygen-containing functional groups and its regeneration. *Adsorption Science & Technology*, **37**(1-2); 160–181

Lee, I., G. H. Jeong, S. An, S.-W. Kim, and S. Yoon (2018). Facile synthesis of 3D MnNi-layered double hydroxides (LDH)/graphene composites from directly graphites for pseudocapacitor and their electrochemical analysis. *Applied Surface Science*, **429**; 196–202

Lesbani, A., N. R. Palapa, R. J. Sayeri, T. Taher, and N. Hidayati (2021). High Reusability of NiAl LDH/Biochar Composite in the Removal Methylene Blue from Aqueous Solution. *Indonesian Journal of Chemistry*

Lesbani, A. L., N. Normah, N. R. Palapa, T. Taher, R. Andreas, and R. Mohadi (2020). Removal of Iron(II) Using Ni/Al Layered Double Hydroxide Intercalated with Keggin Ion. *Molekul*, **15**(3); 149

Linghu, W., H. Yang, Y. Sun, G. Sheng, and Y. Huang (2017a). One-pot synthesis of LDH/GO composites as highly effective adsorbents for decontamination of U (VI). *ACS Sustainable Chemistry & Engineering*, **5**(6); 5608–5616

Linghu, W., H. Yang, Y. Sun, G. Sheng, and Y. Huang (2017b). One-Pot Synthesis of LDH/GO Composites as Highly Effective Adsorbents for Decontamination of U(VI). *ACS Sustainable Chemistry & Engineering*, **5**(6); 5608–5616

Lyu, H., K. Hu, J. Fan, Y. Ling, Z. Xie, and J. Li (2020). 3D hierarchical layered double hydroxide/carbon spheres composite with hollow structure for high adsorption of dye. *Applied Surface Science*, **500**; 144037

Mon, E. E. (2018). Study on the Silica from Rice Husk Ash by XRD and XRF. *Int. J. Sci. Eng. Res*, **9**(6); 1535–1537

Mostafa, M., A. Bakr, G. Eshaq, and M. Kamel (2014). Novel Co/Mo layered double hydroxide: synthesis and uptake of Fe(II) from aqueous solutions (Part 1). *Desalination and Water Treatment*, **56**(1); 239–247

Palapa, N. R., R. Mohadi, A. Rachmat, et al. (2020a). Adsorption study of malachite green removal from aqueous solution using Cu/M3+ (M3+= Al, Cr) layered double hydroxide. *Mediterranean Journal of Chemistry*, **10**(1); 33–45

Palapa, N. R., T. Taher, R. Mohadi, A. Rachmat, and A. Lesbani (2020b). Preparation of copper aluminum-biochar composite as adsorbent of malachite green in aqueous solution. *Chemical Physics*

Palapa, N. R., T. Taher, B. R. Rahayu, R. Mohadi, A. Rachmat, and A. Lesbani (2020c). CuAl LDH/Rice Husk Biochar Composite for Enhanced Adsorptive Removal of Cationic Dye from Aqueous Solution. *Bulletin of Chemical Reaction Engineering & Catalysis*, **15**(2); 525–537

Palapa, N. R., T. Taher, B. R. Rahayu, R. Mohadi, A. Rachmat, and A. Lesbani (2020d). CuAl LDH/Rice Husk Biochar Composite for Enhanced Adsorptive Removal of Cationic Dye from Aqueous Solution. *Bulletin of Chemical Reaction Engineering & Catalysis*, **15**(2); 525–537

Radnia, H., A. A. Ghoreyshi, H. Younesi, and G. D. Najafpour (2012). Adsorption of Fe(II) ions from aqueous phase by chitosan adsorbent: equilibrium, kinetic, and thermodynamic studies. *Desalination and Water Treatment*, **50**(1-3); 348–359

Ravuru, S. S., A. Jana, and S. De (2019). Synthesis of NiAl-layered double hydroxide with nitrate intercalation: Application in cyanide removal from steel industry effluent. *Journal of Hazardous Materials*, **373**; 791–800

Shrestha, S. L. (2018). Study of the Adsorption Kinetics of Iron Ion from Wastewater Using Banana Peel. *International Journal of Advanced Research Chemical Science*, **5**(3); 1–8

Siregar, P. M. S. B. N., N. R. Palapa, A. Wijaya, E. S. Fitri, and A. Lesbani (2021). Structural Stability of Ni/Al Layered Double Hydroxide Supported on Graphite and Biochar Toward Adorption of Congo Red. *Science and Technology Indonesia*, **6**(2); 85–95

Taher, T., M. M. Christina, M. Said, N. Hidayati, F. Ferlinahayati, and A. Lesbani (2019). Removal of iron (II) using intercalated Ca/Al layered double hydroxides with [α-SiW12O40] 4. *Bulletin of Chemical Reaction Engineering & Catalysis*, **14**(2); 260–267

Tan, Y., X. Yin, C. Wang, H. Sun, A. Ma, G. Zhang, and N. Wang (2019). Sorption of cadmium onto Mg-Fe Layered Double Hydroxide (LDH)-Kiwi branch biochar. *Environmental Pollutants and Bioavailability*, **31**(1); 189–197

Tang, Z., Z. Qiu, S. Lu, and X. Shi (2020). Functionalized layered double hydroxide applied to heavy metal ions absorption: A review. *Nanotechnology Reviews*, **9**(1); 800–819

Tyas, A. H., T. A. Zaharah, and A. Shofiyani (2018). Penentuan Kemampuan Penggunaan Ulang Komposit Kitosan-Karbon pada Proses Adsorpsi Ce (IV). *Jurnal Kimia Khatulistiwa*, **7**(2)

Wang, L., A. Li, and Y. Chang (2016). Hydrothermal treatment coupled with mechanical expression at increased temperature for excess sludge dewatering: Heavy metals, volatile organic compounds and combustion characteristics of hydrochar. *Chemical Engineering Journal*, **297**; 1–10

Wazir, A. H., I. U. Wazir, and A. M. Wazir (2020). Preparation and characterization of rice husk based physical activated carbon. *Energy Sources, Part A: Recovery, Utilization, and Environmental Effects*; 1–11

Zhang, Y., J. Zhao, Z. Jiang, D. Shan, and Y. Lu (2014). Biosorption of Fe(II) and Mn(II) Ions from Aqueous Solution by Rice Husk Ash. *BioMed Research International*, **2014**; 1–10

Zubair, M., M. Daud, G. McKay, F. Shehzad, and M. A. Al-Harthi (2017). Recent progress in layered double hydroxides (LDH)-containing hybrids as adsorbents for water remediation. *Applied Clay Science*, **143**; 279–292